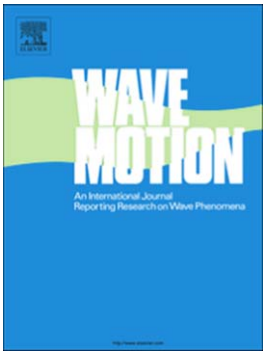

High frequency analysis of the efficiency of a local approximate DtN2 boundary condition for prolate spheroidal-shaped boundaries

H. Barucq, R. Djellouli, A. Saint-Guirons

PII: S0165-2125(10)00053-3
DOI: doi: 10.1016/j.wavemoti.2010.04.004
Reference: WAMOT 1527

To appear in: *Wave Motion*

Received date: 11 December 2009
Revised date: 19 April 2010
Accepted date: 28 April 2010

Please cite this article as: H. Barucq, R. Djellouli, A. Saint-Guirons, High frequency analysis of the efficiency of a local approximate DtN2 boundary condition for prolate spheroidal-shaped boundaries, *Wave Motion* (2010), doi: 10.1016/j.wavemoti.2010.04.004

High frequency analysis of the efficiency of a local approximate DtN2 boundary condition for prolate spheroidal-shaped boundaries

H. Barucq[1,2], R.Djellouli[3,1], A. Saint-Guirons[4]

[1] *Team-project MAGIQUE-3D, INRIA Research Center of Bordeaux Sud-Ouest*
[2] *Laboratoire de Mathématiques Appliquées, CNRS UMR 5142, Université de Pau et des Pays de l'Adour, IPRA-Avenue de l'Université, 64013 Pau, France*
[3] *Department of Mathematics, California State University Northridge, CA 91330-8313, USA*
[4] *Basque Center for Applied Mathematics, Bizkaia Technology Park, Building 500. 48160 Derio Spain*

Abstract

The performance of the second order local approximate DtN boundary condition suggested in [4] is investigated *analytically* when employed for solving high-frequency exterior Helmholtz problems with elongated scatterers. This study is performed using a domain-based formulation and assuming the scatterer and the exterior artificial boundary to be prolate spheroid. The analysis proves that, in the high frequency regime, the reflected waves at the artificial boundary decay faster than $1/(ka)^{15/8}$, where k is the wavenumber and a is the semi-major axis of this boundary. Numerical results are presented to illustrate the accuracy and the efficiency of the proposed absorbing boundary condition, and to provide guidelines for satisfactory performance.

Key words: acoustic scattering problems, elliptic coordinates, prolate spheroidal-shaped boundaries, absorbing boundary conditions, DtN operator.

1 Introduction

The development of efficient solution methodologies for solving scattering problems is very important to many applications such as sonar, radar, medical

Email address: helene.barucq@univ-pau.fr, rabia.djellouli@csun.edu, saint-guirons@bcamath.org (H. Barucq[1,2], R.Djellouli[3,1], A. Saint-Guirons[4]).

imaging, geophysical exploration, non destructive testing, etc. This is a very challenging problem because of two difficulties that one need to address: (a) the discretization issue related to the wavenumber, especially in the high frequency regime, and (b) the unboundness nature of the computational domain (see, for example, the recent monograph [16] and the references therein) . In this work, we focus on the second aspect of this problem and we consider one of the basic problem in the scattering theory: the scattering of time-harmonic acoustic waves by a bounded impenetrable obstacle [8]. The computation of the corresponding acoustic scattered field when using finite element methods, requires first to reformulate this class of problems in a finite domain by surrounding the scatterer by an artificial boundary. The main difficulty here is the construction of a simple but reliable as well as cost-effective absorbing boundary condition for representing the far-field behavior of the scattered field on the prescribed artificial boundary. Various absorbing boundary conditions have been suggested for over seventy years to address this challenging and important issue, and the quest for efficient nonreflecting conditions is still ongoing (see, for example, the latest review by Turkel in [24]).

Recently, a new class of absorbing boundary conditions called local approximate DtN absorbing boundary conditions (DtN) has been proposed to be applied on exterior artificial prolate spheroidal-shaped boundaries [4]. Unlike the standard approximate local DtN boundary conditions that are restricted to circular- or spherical-shaped boundaries (see [11],[12]), the proposed conditions are applicable to exterior elliptical- or prolate spheroidal-shaped boundaries that are more suitable for surrounding elongated scatterers because they yield to smaller computational domains. These absorbing boundary conditions are designed to be exact for the first modes. They can be easily incorporated in any finite element parallel code while preserving the local structure of the algebraic system. Moreover, the analysis of the performance of these conditions in the *low* frequency regime, when using an On-Surface radiation condition formulation [15], revealed that these conditions are very accurate regardless of the slenderness of the boundary [4],[23]. In addition, it has been demonstrated that the *second-order* local DtN condition (DtN2) outperforms the widely-used second-order absorbing boundary conditions (BGT2) [6] when expressed in prolate spheroidal coordinates [21],[22]. Note that the derivation of the considered DtN2 boundary condition is slightly different then the absorbing boundary condition proposed in [17]. Moreover, when the eccentricity of the boundary tends to zero ($e \to 0$) our condition coincides with the standard BGT2/DtN2 condition for spherical-shaped boundaries, as shown in [4],[23].

We propose to extend the investigation of the performance of the local approximate DtN2 absorbing boundary condition to the case of the *high*-frequency regime. The objective of this analytical study is to shed some light on the potential of this new class of boundary conditions for solving efficiently high-frequency acoustic scattering problems in the case of elongated scatterers, and

to provide practical guidelines for avoiding excessive computational cost when employed for practical applications. More specifically, we perform an analytical and a numerical investigation to assess the effect of the slenderness of the exterior boundary as well as its distance from the scatterer on the accuracy and the efficiency of the proposed absorbing boundary condition in the high-frequency regime. We conduct this study using a domain-based formulation, that is the artificial boundary is located at some distance from the surface of the scatterer, since the OSRC approach is not adapted for such an analysis, as previously observed in [2]. Such an analysis is conducted in the case of the *canonical* boundary value problem, i.e. the scatterer is assumed to be prolate spheroid. We must point out that considering the *canonical* boundary value problem is a standard approach for assessing the performance of absorbing boundary conditions [13],[21] and/or for improving their performance [21],[3]. This study is a first and important step to highlight the potential of the proposed boundary condition for solving efficiently high-frequency acoustic scattering problems in the case of elongated scatterers. Note that the numerical investigation of the performance of this condition for arbitrarily-shaped scatterers using other approaches such as finite element/finite difference-based formulations will incur numerical errors due to the discretization scheme. In the high-frequency regime, the range of our interest, these discretization errors are not avoidable, and may even be very important. The use of an "overkilled" mesh along with the use of the exterior boundary very far from the scatterer, to compute a *reliable* reference solution may simply not be possible in the high-frequency regime due to the prohibitive computational cost. Therefore, it would be very difficult to distinguish between the errors due to the boundary condition and the discretization scheme. Consequently it would be very hard –if not impossible– to draw a meaningful conclusion on the performance of the proposed boundary condition.

The remainder of this paper is as follows. In Section 2, we specify the nomenclature and assumptions, and formulate the considered three-dimensional acoustic scattering problem in a bounded domain using the local approximate DtN2 absorbing boundary condition proposed in [4]. The main results of this work are established in Section 3. More specifically, we analyze the mathematical properties of the solution of the *canonical* boundary value problem in the high-frequency regime. We prove the existence and the uniqueness of the solution. This *stability* result ensures the well-posedness of the canonical boundary value problem in the high-frequency regime regardless of the location and the eccentricity values of the exterior boundary. The accuracy of the proposed boundary is performed by analyzing the asymptotic behavior of the Fourier coefficients of the solution. This analysis reveals that the reflected waves at the artificial boundary decay faster than $1/(ka)^{15/8}$, where k is the wavenumber and a is the semi-major axis of this boundary. This quasi-quadratic decay of the reflected waves with respect to the wavenumber values ka, suggests that the exterior boundary could be positioned at a very small distance from the

surface of the scatterer, as illustrated by the numerical reported in this section, to achieve an acceptable level of accuracy. This observation illustrates the potential of the proposed boundary condition for reducing the size of the computational domain for elongated scatterers. Concluding remarks are discussed in Section 4. The particular case of the absorbing boundary condition BGT2 when employed on spherical-shaped exterior boundaries is discussed in the Appendix.

2 Preliminaries

2.1 Nomenclature and assumption

Throughout this paper, we use the prolate spheroidal coordinates (ξ, φ, θ), related to the cartesian coordinates (x, y, z) by $x = b \sin\varphi \cos\theta$, $y = b \sin\varphi \sin\theta$, and $z = a \cos\varphi$, where $\varphi \in [0, \pi)$ and $\theta \in [0, 2\pi)$i (see Fig.1). The parameters a and b are the semi-major and the semi-minor axes respectively, and are given by $a = f \cosh\xi$ and $b = f \sinh\xi$ where ξ is strictly positive and the real number f is the interfocal distance ($f = \sqrt{a^2 - b^2}$).

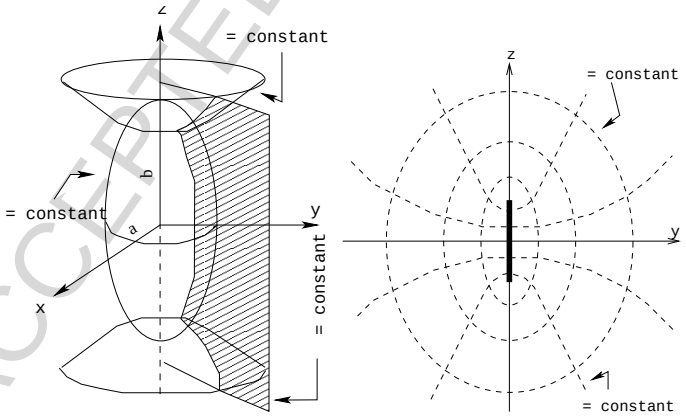

Fig. 1. The prolate spheroidal coordinates.

In addition, we adopt the following notations:

- k is a positive number representing the wavenumber.
- $R_{mn}^{(j)}(kf, \cosh\xi)$ is the radial spheroidal wave function of the j^{th} kind corresponding to the $(mn)^{\text{th}}$(see p. 30 in [10]) where $(m, n) \in \mathbb{N}^2$ such that $n \geq m$.
- $S_{mn}(kf, \cos\varphi)$ is the angular spheroidal wave function corresponding to the $(mn)^{\text{th}}$ mode (see p. 16 in [10]).
- N_{mn} is the normalization factor associated to $S_{mn}(kf, \cos\varphi)$. N_{mn} is given

by (see Eq. (3.1.32) p. 22 in [10]):

$$N_{mn} = \int_{-1}^{1} \left[S_{mn}\left(kf, v\right)\right]^2 \, dv \tag{1}$$

- λ_{mn} is the prolate spheroidal eigenvalue (see p. 11 in [10]).
- Ω is a prolate spheroidal-shaped scatterer whose surface is denoted by Γ. Ω^e is the open complement in $\mathbb{R}^3$ of the domain $\overline{\Omega}$.

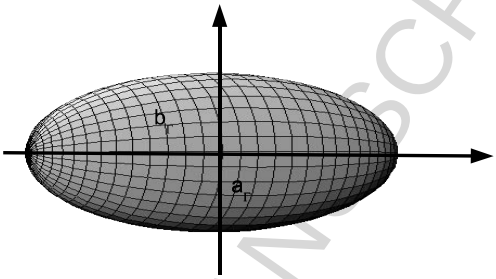

Fig. 2. A prolate spheroidal-shaped scatterer Ω.

- a_Γ (resp. b_Γ) represents the semi-major (resp. semi-minor) axis of the scatterer Ω. e_Γ is the eccentricity
- Σ is an artificial boundary surrounding the scatterer Ω. Σ is assumed to be a prolate-spheroid surface.

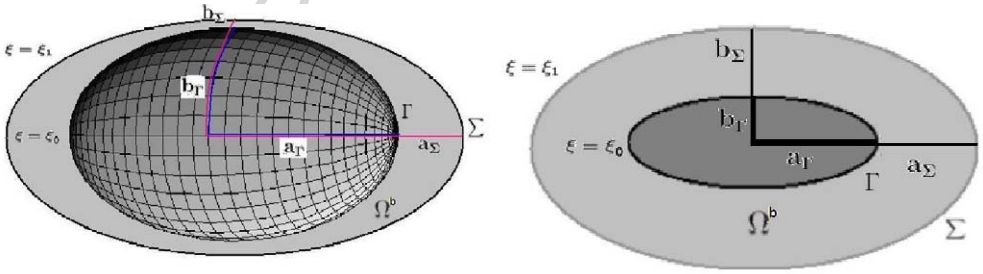

Fig. 3. Geometry of the bounded computational domain Ω^b (left) with a two-dimensional illustration in the xy-plane (right).

- a_Σ (resp. b_Σ) is the semi-major (resp. semi-minor) axis of the prolate spheroidal-shaped domain whose surface is Σ. e_Σ is its eccentricity.
- Ω^b is a bounded computational domain whose interior (resp. exterior) boundary is Γ (resp. Σ).
- Δ_Σ is the Laplace Beltrami operator on Σ.
- For a function F_{mn}, we denote its restriction on Γ by:

$$F_{mn_{|\Gamma}} = F_{mn}\left(e_\Gamma k a_\Gamma, e_\Gamma^{-1}\right) \tag{2}$$

Similarly, the restriction of F_{mn} on Σ is denoted by:

$$F_{mn_{|\Sigma}} = F_{mn}\left(e_\Sigma k a_\Sigma, e_\Sigma^{-1}\right) \tag{3}$$

- The partial derivative of the radial spheroidal wave function $R_{mn}^{(j)}$ with respect to the variable ξ is denoted by $R_{mn}^{(j)\prime}$, i.e.

$$R_{mn}^{(j)\prime} = \frac{\partial R_{mn}^{(j)}}{\partial \xi};\ \ j =\in \mathbb{N} \tag{4}$$

- $r_{mn|_\Sigma}$ are complex numbers given by:

$$r_{mn_{|\Sigma}} = \frac{R_{mn_{|\Sigma}}^{(3)\prime}}{R_{mn_{|\Sigma}}^{(3)}} \tag{5}$$

- $r_{mn_{|\Sigma}}^{(j)}$ are complex numbers given by:

$$r_{mn_{|\Sigma}}^{(j)} = \begin{cases} \dfrac{R_{mn_{|\Sigma}}^{(3)\prime}}{R_{mn_{|\Sigma}}^{(3)}} & \text{if } j = 3 \\ \\ \dfrac{R_{mn_{|\Sigma}}^{(4)\prime}}{R_{mn_{|\Sigma}}^{(4)}} & \text{if } j = 4 \end{cases} \tag{6}$$

  Note that it follows from (5) and (6) that $r_{mn_{|\Sigma}}^{(3)} = r_{mn_{|\Sigma}}$
- $||.||_2$ is the euclidean norm.

2.2 The acoustic scattering problem

Recall that the direct acoustic scattering problem by a sound-soft scatterer Ω can be formulated as follows [**?**]:

$$\begin{cases} \Delta u^{\text{scat}} + k^2 u^{\text{scat}} = 0 & \text{in } \Omega^e \\ \\ u^{\text{scat}} = -u^{\text{inc}} & \text{on } \Gamma \\ \\ \lim\limits_{||x||_2 \to +\infty} ||x||_2 \left[\dfrac{\partial u^{\text{scat}}}{\partial ||x||_2} - \mathrm{i}k u^{\text{scat}}\right] = 0 \end{cases} \tag{7}$$

where Δ is the Laplace operator, u^{scat} is the scattered field, and u^{inc} is the incident plane wave. Note that u^{inc} can be expressed, in prolate spheroid co-

ordinates, as an infinite series (see Eq. (7) p. 233 in [20]):

$$u^{\text{inc}} = \sum_{m=0}^{+\infty} \sum_{n=m}^{+\infty} d_{mn}^{\text{inc}}\, u_{mn}^{(1)}\left(kf, \cosh\xi, \cos\varphi\right) \tag{8}$$

where the mn^{th} Fourier mode $u_{mn}^{(j)}$ is given by:

$$u_{mn}^{(j)}\left(kf, \cosh\xi, \cos\varphi\right) = R_{mn}^{(j)}\left(kf, \cosh\xi\right) \frac{S_{mn}\left(kf, \cos\varphi\right)}{\sqrt{N_{mn}}} \cos m\theta, \text{ for } j \in \mathbb{N}. \tag{9}$$

and the mn^{th} Fourier coefficient d_{mn}^{inc} is given by:

$$d_{mn}^{\text{inc}} = 2\varepsilon_m \frac{\mathrm{i}^n}{\sqrt{N_{mn}}} S_{mn}\left(kf, \cos\varphi_0\right) \tag{10}$$

φ_0 is the incident angle of the plane wave u^{inc}, $\varepsilon_m = (2 - \delta_{0m})$, and δ_{0m} is the Kronecker symbol.

Furthermore, the solution u^{scat} of the exterior boundary value problem (7) , in the case where Ω is a prolate spheroidal-shaped scatterer (see Fig. 2), can be expressed as an infinite series (see Eq. (11.36) p. 422 in [7]):

$$u^{\text{scat}} = \sum_{m=0}^{+\infty} \sum_{n=m}^{+\infty} d_{mn}^{scat}\, u_{mn}^{(3)}\left(kf, \cosh\xi, \cos\varphi\right) \tag{11}$$

where the mn^{th} Fourier outgoing mode $u_{mn}^{(3)}\left(kf, \cosh\xi, \cos\varphi\right)$ is given by Eq. (9), whereas the mn^{th} Fourier coefficient d_{mn}^{scat} is given by:

$$d_{mn}^{\text{scat}} = -2\varepsilon_m \frac{\mathrm{i}^n}{\sqrt{N_{mn}}} \frac{R_{mn_{|\Gamma}}^{(1)}}{R_{mn_{|\Gamma}}^{(3)}} S_{mn}\left(e_\Gamma k a_\Gamma, \cos\varphi_0\right) \tag{12}$$

Observe that it follows from substituting Eq.(10) into Eq.(12) that:

$$d_{mn}^{\text{scat}} = -\frac{R_{mn_{|\Gamma}}^{(1)}}{R_{mn_{|\Gamma}}^{(3)}} d_{mn_{|\Gamma}}^{\text{inc}} \tag{13}$$

Note that the Dirichlet boundary condition, characterizing sound-soft scatterers, is used in the boundary value problem (7) for simplicity only. Analytical expressions for other boundary conditions can be also derived [7].

2.3 Bounded domain-based formulation

The application of finite element techniques when solving numerically the exterior boundary value problem (7) requires first to set it in a bounded do-

main. This is achieved, in the nonreflecting boundary conditions context, by surrounding the scatterer Ω with an artificial boundary Σ and prescribing a so-called absorbing boundary condition. Consequently, when setting on Σ the second-order local approximate DtN boundary condition suggested in [4], the exterior acoustic scattering problem (7) is reformulated in the bounded domain Ω^b as follows:

$$\begin{cases} \Delta u^{\mathrm{DtN}} + k^2 u^{\mathrm{DtN}} = 0 & \text{in } \Omega^b \\ u^{\mathrm{DtN}} = -u^{\mathrm{inc}} & \text{on } \Gamma \\ \dfrac{\partial u^{\mathrm{DtN}}}{\partial \mathbf{n}} = \dfrac{1}{a_\Sigma \sqrt{1 - e_\Sigma^2 \cos^2 \varphi}} T u^{\mathrm{DtN}} & \text{on } \Sigma \end{cases} \tag{14}$$

where $\mathbf{n}$ is the outward normal to the exterior boundary Σ, and T is the second-order local approximate DtN operator expressed in prolate spheroid coordinates as follows [4]:

$$\begin{aligned} Tu = \frac{\sqrt{1 - e_\Sigma^2}}{\left(\lambda_{01_{|\Sigma}} - \lambda_{00_{|\Sigma}}\right) e_\Sigma} \Big\{ \Big[& \lambda_{01_{|\Sigma}} r_{01_{|\Sigma}} - \lambda_{00_{|\Sigma}} r_{00_{|\Sigma}} \\ & - \left(r_{00_{|\Sigma}} - r_{01_{|\Sigma}}\right) \left(e_\Sigma k a_\Sigma\right)^2 \cos^2 \varphi \Big] u \\ & + \left(r_{00_{|\Sigma}} - r_{01_{|\Sigma}}\right) \Delta_\Sigma u \Big\} \end{aligned} \tag{15}$$

Note that the field u^{DtN} is an *approximation* of the scattered field u^{scat}. We analyze the property of the approximate solution u^{DtN} for the *canonical* boundary value problem, that is we assume the scatterer Ω to be prolate spheroid (see Fig.2). The computational domain Ω^b is the exterior domain to Ω bounded by the artificial boundary Σ, as depicted in Fig. 3. The goal of this analytical study is to shed some light on the potential of the absorbing boundary condition (15) for solving efficiently high frequency acoustic scattering problems, and to provide practical guidelines for avoiding excessive computations.

3 Analytical study

We analyze the mathematical properties of the solution of the *canonical* boundary value problem (14) in the high frequency. We also assess the efficiency of the second-order local approximate DtN boundary condition given by Eq. (15). Numerical results are presented for illustration.

3.1 Existence and uniqueness of the approximate solution

We investigate in this section the well-posedness nature of the *canonical* boundary value problem (14). We state a necessary and sufficient condition to ensure the existence and the uniqueness of the solution u^{DtN}, and illustrate numerically this study.

3.1.1 Mathematical results

The approximate scattered field u^{DtN} can be expressed as an infinite series of outgoing modes $R_{mn}^{(3)}(kf, \cosh\xi))$ and incoming modes $R_{mn}^{(4)}(kf, \cosh\xi))$. More specifically, we have (see Eq. (16) p. 233 in [20]):

$$u^{\mathrm{DtN}} = \sum_{m=0}^{+\infty} \sum_{n=m}^{+\infty} \left[d_{mn}^{\mathrm{DtN}} u_{mn}^{(3)}(kf, \cosh\xi, \cos\varphi) + \tau_{mn}^{\mathrm{DtN}} u_{mn}^{(4)}(kf, \cosh\xi, \cos\varphi) \right] \tag{16}$$

where $u_{mn}^{(j)}(kf, \cosh\xi, \cos\varphi)$ are given by Eq. (9).

The incoming waves are the reflections of the scattered field due to the presence of the artificial exterior boundary Σ. Note that in the case of a perfectly nonreflecting boundary condition, the Fourier coefficients must satisfy $\tau_{mn}^{\mathrm{DtN}} = 0$ and $d_{mn}^{\mathrm{DtN}} = d_{mn}^{\mathrm{scat}}$ for all $(m,n) \in \mathbb{N}^2$ such that $n \geq m$. Therefore, the degree of transparency of any absorbing boundary condition, and thus the level of accuracy in the approximation as well as the computational cost, depend on (a) the magnitude of the reflection coefficients $|\tau_{mn}^{\mathrm{DtN}}|$ of the incoming waves, and (b) the magnitude of the difference $|d_{mn}^{\mathrm{DtN}} - d_{mn}^{\mathrm{scat}}|$. These two quantities become very small (resp. very large) as the intensity of the reflected waves at the boundary Σ are negligible (resp. very important).

Next, we investigate the properties of these coefficients. We first define, for all $(m,n) \in \mathbb{N}^2$ such that $n \geq m$, the following wronskian-like expression:

$$W_{mn}^{3,4}(\Gamma, \Sigma) = R_{mn_{|\Gamma}}^{(3)} \Psi_{mn_{|\Sigma}}^{(4)} - R_{mn_{|\Gamma}}^{(4)} \Psi_{mn_{|\Sigma}}^{(3)} \tag{17}$$

where

$$\Psi_{mn_{|\Sigma}}^{(j)} = R_{mn_{|\Sigma}}^{(j)} \left[c_{mn_{|\Sigma}} + r_{mn_{|\Sigma}}^{(j)} \right], \text{ for } j = 3, 4. \tag{18}$$

8

and

$$c_{mn_{|\Sigma}} = \frac{r_{00_{|\Sigma}} \left(\lambda_{01_{|\Sigma}} - \lambda_{mn_{|\Sigma}} \right) - r_{01|\Sigma} \left(\lambda_{00_{|\Sigma}} - \lambda_{mn_{|\Sigma}} \right)}{\lambda_{00_{|\Sigma}} - \lambda_{01_{|\Sigma}}} \tag{19}$$

Observe that when $\Sigma \equiv \Gamma$, Eq. (17) is the standard wronskian between $R^{(3)}_{mn_{|\Gamma}}$ and $R^{(4)}_{mn_{|\Gamma}}$.

The following result pertains to the existence and uniqueness of the Fourier coefficients d^{DtN}_{mn} and τ^{DtN}_{mn}.

Theorem 3.1 *The approximate scattered field u^{DtN}, solution of the boundary value problem* (14)*, exists and is unique if and only if*

$$W^{3,4}_{mn}(\Gamma,\Sigma) \neq 0 \quad \forall\,(m,n) \in \mathbb{N}^2, n \geq m \tag{20}$$

Moreover, if condition (20) *is satisfied, then the Fourier coefficients d^{DtN}_{mn} and τ^{DtN}_{mn} are given by:*

$$\begin{cases} d^{\mathrm{DtN}}_{mn} = \dfrac{\Psi^{(4)}_{mn_{|\Sigma}} R^{(3)}_{mn_{|\Gamma}}}{W^{3,4}_{mn}(\Gamma,\Sigma)}\, d^{\mathrm{scat}}_{mn} \\[2ex] \tau^{\mathrm{DtN}}_{mn} = \dfrac{\Psi^{(3)}_{mn_{|\Sigma}} R^{(3)}_{mn_{|\Gamma}}}{W^{3,4}_{mn}(\Gamma,\Sigma)}\, d^{\mathrm{scat}}_{mn} \end{cases} \tag{21}$$

Proof of Theorem 3.1. First, we substitute the Fourier series representations of both the approximate scattered field u^{DtN} given by Eq.(16) and the incident plane wave u^{inc} given by Eq.(8) into the boundary conditions of the boundary value problem (14). Consequently, for all $(m,n) \in \mathbb{N}^2$ such that $n \geq m$, we have:

$$\begin{cases} d^{\mathrm{DtN}}_{mn} R^{(3)}_{mn_{|\Gamma}} + \tau^{\mathrm{DtN}}_{mn} R^{(4)}_{mn_{|\Gamma}} = -d^{\mathrm{inc}}_{mn} R^{(1)}_{mn_{|\Gamma}} & \text{on } \Gamma \\[2ex] d^{\mathrm{DtN}}_{mn} \Psi^{(3)}_{mn_{|\Sigma}} + \tau^{\mathrm{DtN}}_{mn} \Psi^{(4)}_{mn_{|\Sigma}} = 0 & \text{on } \Sigma \end{cases} \tag{22}$$

The linear 2×2 system (22) is invertible if and only if the condition (20) is satisfied, and we have:

$$\begin{cases} d^{\mathrm{DtN}}_{mn} = -\dfrac{d^{\mathrm{inc}}_{mn} \Psi^{(4)}_{mn_{|\Sigma}} R^{(1)}_{mn_{|\Gamma}}}{W^{3,4}_{mn}(\Gamma,\Sigma)} \\[2ex] \tau^{\mathrm{DtN}}_{mn} = \dfrac{d^{\mathrm{inc}}_{mn} \Psi^{(3)}_{mn_{|\Sigma}} R^{(1)}_{mn_{|\Gamma}}}{W^{3,4}_{mn}(\Gamma,\Sigma)} \end{cases} \tag{23}$$

We then conclude the proof of Theorem 3.1 by substituting Eq. (13) into Eq. (23).

□

Remark 3.2 *Note that using Eqs.* (17)-(19) *for* $n = 0, 1$*, leads to:*

$$\Psi^{(3)}_{0n_{|\Sigma}} = 0 \quad \text{and} \quad W^{3,4}_{0n}(\Gamma, \Sigma) = \Psi^{(4)}_{0n_{|\Sigma}} R^{(3)}_{0n_{|\Gamma}}$$

Consequently, it follows from Theorem 3.1 that the Fourier coefficients corresponding to the first two modes satisfy:

$$d^{\mathrm{DtN}}_{0n} = d^{\mathrm{scat}}_{0n} \quad \text{and} \quad \tau^{\mathrm{DtN}}_{0n} = 0 \ ; \quad n = 0, 1 \tag{24}$$

Hence, Theorem 3.1 states that the first two modes in the infinite series given by Eq. (16) *are the exact modes propagating towards the infinity and do not reflect at the artificial boundary* Σ*. This result is not surprising since the second-order local approximate DtN boundary condition given by Eq.* (15) *was constructed to be exact for the first two modes [4].*

Next, we analyze the properties of the $W^{3,4}_{mn}(\Gamma, \Sigma)$ to determine when condition (20) is fullfilled. The result below describes the asymptotic behavior of $W^{3,4}_{mn}(\Gamma, \Sigma)$ as $ka_\Gamma \to \infty$.

Proposition 3.3 *For all* $(m, n) \in \mathbb{N}^2$ *such that* $n \geq m$*, the wronskian-like function* $W^{3,4}_{mn}(\Gamma, \Sigma)$ *given by Eq.*(17) *satisfies:*

$$W^{3,4}_{mn}(\Gamma, \Sigma) \sim -\frac{2\,\mathrm{i}\,e_\Sigma}{ka_\Gamma}\, e^{\mathrm{i}\,k(a_\Gamma - a_\Sigma)} \ ; \quad \text{as} \quad ka_\Gamma \to \infty \tag{25}$$

Proof of Proposition 3.3. First, we use Eqs.(17)-(19), and rewrite $W^{3,4}_{mn}(\Gamma, \Sigma)$ as follows:

$$\begin{aligned} W^{3,4}_{mn}(\Gamma, \Sigma) = {} & R^{(3)}_{mn_{|\Gamma}} R^{(4)}_{mn_{|\Sigma}} r^{(4)}_{mn_{|\Sigma}} - R^{(4)}_{mn_{|\Gamma}} R^{(3)}_{mn_{|\Sigma}} r^{(3)}_{mn_{|\Sigma}} \\ & + c_{mn} \left[R^{(3)}_{mn_{|\Gamma}} R^{(4)}_{mn_{|\Sigma}} - R^{(4)}_{mn_{|\Gamma}} R^{(3)}_{mn_{|\Sigma}} \right] \end{aligned} \tag{26}$$

Next, we analyze the asymptotic behavior of each term in Eq. (26). Observe that when $ka_\Gamma \to \infty$, then necessarily $ka_\Sigma \to \infty$.
We have (see Eqs. (21.9.4)-(21.9.5) p. 756 in [1]):

$$R^{(3)}_{mn_{|\bullet}} \sim \overline{R^{(4)}_{mn_{|\bullet}}} \sim \frac{1}{ka_\bullet} \mathrm{e}^{\mathrm{i}\left(ka_\bullet - \frac{1}{2}(n+1)\pi\right)} \ ; \quad ka_\bullet \to +\infty \tag{27}$$

where the symbole $\bullet$ can be either Γ or Σ and the overline denotes the complex conjugate.
From Eq. (6) and Eq. 4.1.16, p. 32 in [10] (or Eq. 80 p. 3647 in [21]) , we deduce that for $j = 3, 4$:

$$r^{(j)}_{mn_{|\Sigma}} \sim e_\Sigma ka_\Sigma \, \frac{h^{(j-2)\prime}_n(ka_\Sigma)}{h^{(j-2)}_n(ka_\Sigma)} \ ; \quad ka_\Sigma \to +\infty \tag{28}$$

where $h_n^{(1)}$ (resp. $h_n^{(2)}$) are the *spherical* Hankel functions of the first (resp. second) kind of order n [1].
On the other hand (see Eq. 10. 1.1 p. 437 [1]), we have

$$\frac{h_n^{(j-2)\prime}(z)}{h_n^{(j-2)}(z)} = \frac{H_{n+1/2}^{(j-2)\prime}(z)}{H_{n+1/2}^{(j-2)}(z)} - \frac{1}{2z} \; ; \quad j = 3, 4 \tag{29}$$

where $H_n^{(1)}$ (resp. $H_n^{(2)}$) are the Hankel functions of the first (resp. second) kind of order n [1].
Then, using the asymptotic behavior of the Hankel functions (see [1]), it follows from Eq.(28) and Eq.(29) that:

$$r^{(3)}_{mn_{|\Sigma}} \sim \overline{r^{(4)}_{mn_{|\Sigma}}} \sim e_\Sigma k a_\Sigma \left[\mathrm{i} - \frac{1}{k a_\Sigma} - \mathrm{i} \frac{n(n+1)}{2} \frac{1}{(k a_\Sigma)^2} \right] \; ; \quad k a_\Sigma \to +\infty \tag{30}$$

Consequently, it follows from Eqs.(26)-Eq.(27) and Eq.(30) that:

$$W^{3,4}_{mn}(\Gamma, \Sigma) \sim 2\,\mathrm{i} \left[\Im(R^{(3)}_{mn_{|\Gamma}} \overline{R^{(3)}_{mn_{|\Sigma}} r^{(3)}_{mn_{|\Sigma}}}) + c_{mn} \Im(R^{(3)}_{mn_{|\Gamma}} \overline{R^{(3)}_{mn_{|\Sigma}}}) \right] \; ; \quad k a_\Gamma \to +\infty \tag{31}$$

Next, we derive the asymptotic behavior of the coefficients c_{mn} given by Eq.(19) as $k a_\Sigma \to +\infty$. To do this, we first recall the asymptotic behavior of the prolate spheroidal eigenvalues $\lambda_{mn_{|\Sigma}}$ as $k a_\Sigma \to +\infty$ (see Eq. 21.7.6 p. 754 in [1]):

$$\lambda_{mn_{|\Sigma}} \sim (2n - 2m + 1)\, e_\Sigma k a_\Sigma \; ; \quad k a_\Sigma \to +\infty \tag{32}$$

Hence, applying the asymptotic behavior given by Eq.(32) together with the asymptotic behavior of $r^{(3)}_{mn_{|\Sigma}}$ for $(m, n) = (0, 0), (0, 1)$ (see Eq. (30)), we deduce that:

$$c_{mn_{|\Sigma}} \sim -e_\Sigma k a_\Sigma \left[\mathrm{i} - \frac{1}{k a_\Sigma} + \mathrm{i}\,(m - n) \frac{1}{(k a_\Sigma)^2} \right] \; ; \quad k a_\Sigma \to +\infty \tag{33}$$

Finally, (25) results from substituting Eq.(27), Eq.(30), and Eq.(33) into Eq.(31). This concludes the proof of Proposition 3.3.

□

Proposition 3.3 states that $|W^{3,4}_{mn}(\Gamma, \Sigma)| \sim \dfrac{2\, e_\Sigma}{k a_\Gamma} \neq 0$ as $k a_\Gamma \to \infty$. Consequently, it follows from Theorem 3.1 the following existence and uniqueness result in the high frequency regime:

Corollary 3.4 *The solution of the boundary value problem* (14) *exists and is unique for large values of* $k a_\Gamma$.

Remark 3.5 *The result stated in Corollary 3.4 proves that the Fourier coefficients* d_{mn}^{DtN} *and* τ_{mn}^{DtN} *always exist and are unique in the high frequency regime regardless of the eccentricity values* e_Σ*, and the location of the exterior boundary* Σ *with respect to* Γ*. This remark shows that the position of the exterior boundary* Σ *is important for the accuracy only.*

The next result addresses the particular case of the first two modes since the proposed absorbing boundary condition is, by construction, exact when applied to them [4].

Proposition 3.6 *The necessary and sufficient condition given by Eq.*(20) *is always satisfied for the first two modes. Furthermore, we have:*

$$W_{0n}^{3,4}(\Gamma,\Sigma) = \frac{R_{0n_\Gamma}^{(3)}}{R_{0n_\Sigma}^{(3)}} \frac{-2\,\mathrm{i}}{e_\Sigma k a_\Sigma (e_\Sigma^{-2}-1)} \;; \quad \text{for } n=0,1 \tag{34}$$

Proof of Proposition 3.6. First, we use Eq.(5) to rewrite the expression of the coefficients $c_{0n_{|\Sigma}}$ $(n=0,1)$ given by Eq. (19) as follows:

$$c_{0n_{|\Sigma}} = -r_{0n_{|\Sigma}} = -\frac{R_{0n_{|\Sigma}}^{(3)\prime}}{R_{0n_{|\Sigma}}^{(3)}} \;; \quad \text{for } n=0,1 \tag{35}$$

Then, for $n=0,1$, we substitute Eq.(6) and Eq.(35) into Eq.(26) and obtain:

$$W_{0n}^{3,4}(\Gamma,\Sigma) = R_{0n_{|\Gamma}}^{(3)} R_{0n_{|\Sigma}}^{(4)\prime} - R_{0n_{|\Gamma}}^{(4)} R_{0n_{|\Sigma}}^{(3)\prime} - \frac{R_{0n_{|\Sigma}}^{(3)\prime}}{R_{0n_{|\Sigma}}^{(3)}} \left[R_{0n_{|\Gamma}}^{(3)} R_{0n_{|\Sigma}}^{(4)} - R_{0n_{|\Gamma}}^{(4)} R_{0n_{|\Sigma}}^{(3)} \right]$$

Thus,

$$W_{0n}^{3,4}(\Gamma,\Sigma) = \frac{R_{0n_{|\Gamma}}^{(3)}}{R_{0n_{|\Sigma}}^{(3)}} W_{0n}^{3,4}(\Sigma) \;; \quad n=0,1 \tag{36}$$

where $W_{0n}^{3,4}(\Sigma)$ is the Wronskian between $R_{0n_{|\Gamma}}^{(3)}$ and $R_{0n_{|\Gamma}}^{(4)}$, that is:

$$W_{0n}^{3,4}(\Sigma) = R_{0n_{|\Sigma}}^{(3)} R_{0n_{|\Sigma}}^{(4)\prime} - R_{0n_{|\Sigma}}^{(4)} R_{0n_{|\Sigma}}^{(3)\prime} \;; \quad n=0,1$$

which can be rewritten, using the representation of $R_{0n_{|\Sigma}}^{(j)}$ $(j=3,4)$ in terms of $R_{0n_{|\Sigma}}^{(l)}$ $(l=1,2)$(see Eq. 4.1.18, p. 32 in [10]), as follows:

$$W_{0n}^{3,4}(\Sigma) = -\,2\,\mathrm{i}\,W_{0n}^{1,2}(\Sigma) \;; \quad n=0,1 \tag{37}$$

Moreover, we have (see Eq. 4.1.21, p. 32 in [10] or Appendix C in [23]):

$$W_{mn}^{1,2}(\Sigma) = \frac{1}{e_\Sigma k a_\Sigma (e_\Sigma^{-2} - 1)} \; ; \quad \forall (m,n) \in \mathbb{N}^2 \quad \text{and } n \geq m \tag{38}$$

Eq.(34) is then an immediate consequence of substituting Eq.(37) and Eq.(38) into Eq.(36).

□

Remark 3.7 *The result stated in Proposition 3.6 proves that the Fourier coefficients* d_{mn}^{DtN} *and* τ_{mn}^{DtN} *corresponding to the first two modes, i. e.* $(m,n) = (0,0),(0,1)$ *exist and are unique independently of the slenderness and the position of the artificial boundary* Σ*, as well on the frequency regime. This property along with the observation made in Remark 3.2 allow to conclude, as expected, that Eq.* (24) *always holds.*

3.1.2 Numerical investigation of the stability condition given by Eq.(20)

Proposition 3.3 proves that the necessary and sufficient condition (20) in Theorem 3.1 is satisfied for all modes but in the high frequency regime only, whereas Proposition 3.6 states that, in the case of the first two modes, this condition holds in all frequency band. Note that these two results are valid with no restriction on the location of the artificial boundary Σ with respect to the boundary Γ of the scatterer Ω.
The objective here is to investigate numerically the validity of condition (20) in the low- and mid-frequency regime. More specifically, we have assumed that the semi-major and semi-minor axes satisfy respectively $a_\Sigma = \sigma\, a_\Gamma$ and $b_\Sigma = \sigma\, b_\Gamma$. The positive real number σ, called the *widening* coefficient, satisfies $\sigma > 1$. Such an assumption implies that the two boundaries have the same eccentricity ($e_\Sigma = e_\Gamma = e$). Note that $\sigma = 1$ corresponds to the extreme case scenario where $\Sigma \equiv \Gamma$, the OSRC formulation [15], [4]. We have analyzed the dependence of $|W_{mn}^{3,4}(\Gamma,\Sigma)|$ with respect to the widening parameter σ. The numerical results reported in [23] tend to indicate that condition (20) holds for all modes and values of ka_Γ with no restriction on the position of Σ. For illustration purpose, we present here (see Figs.(4)-(5)) two sets of results obtained for two frequency values $ka = 10$ and 20, and "very" elongated boundaries $e_\Sigma = e_\Gamma = 0.9$. The results depicted in Figs. (4)-(5) correspond six different modes ranging from the lowest mode $(m,n) = (0,0)$ to a higher mode corresponding to $(m,n) = (7,7)$. The following observations are noteworthy:

- The necessary and sufficient condition (20) is clearly satisfied.
- These results suggest that the Wronskian-like function $|W_{mn}^{3,4}(\Gamma,\Sigma)|$ is an increasing function with respect to the widening parameter σ.
- The results depicted in Figs. (4)-(5), together with those reported in [23],

suggest the following conjecture:

$$|W_{mn}^{3,4}(\Gamma,\Sigma)| \geq \frac{2}{e_\Gamma k a_\Gamma (e_\Gamma^{-2}-1)} \; ; \quad \forall (m,n) \in \mathbb{N}^2 \quad \text{and } n \geq m \tag{39}$$

Note that the lower bound of Eq.(39) corresponds to twice the value of $|W_{mn}^{1,2}(\Gamma)|$ (see Eq. (38)). This conjecture can be easily established in the case of the first two modes (see Eq. (34) in Proposition 3.6).

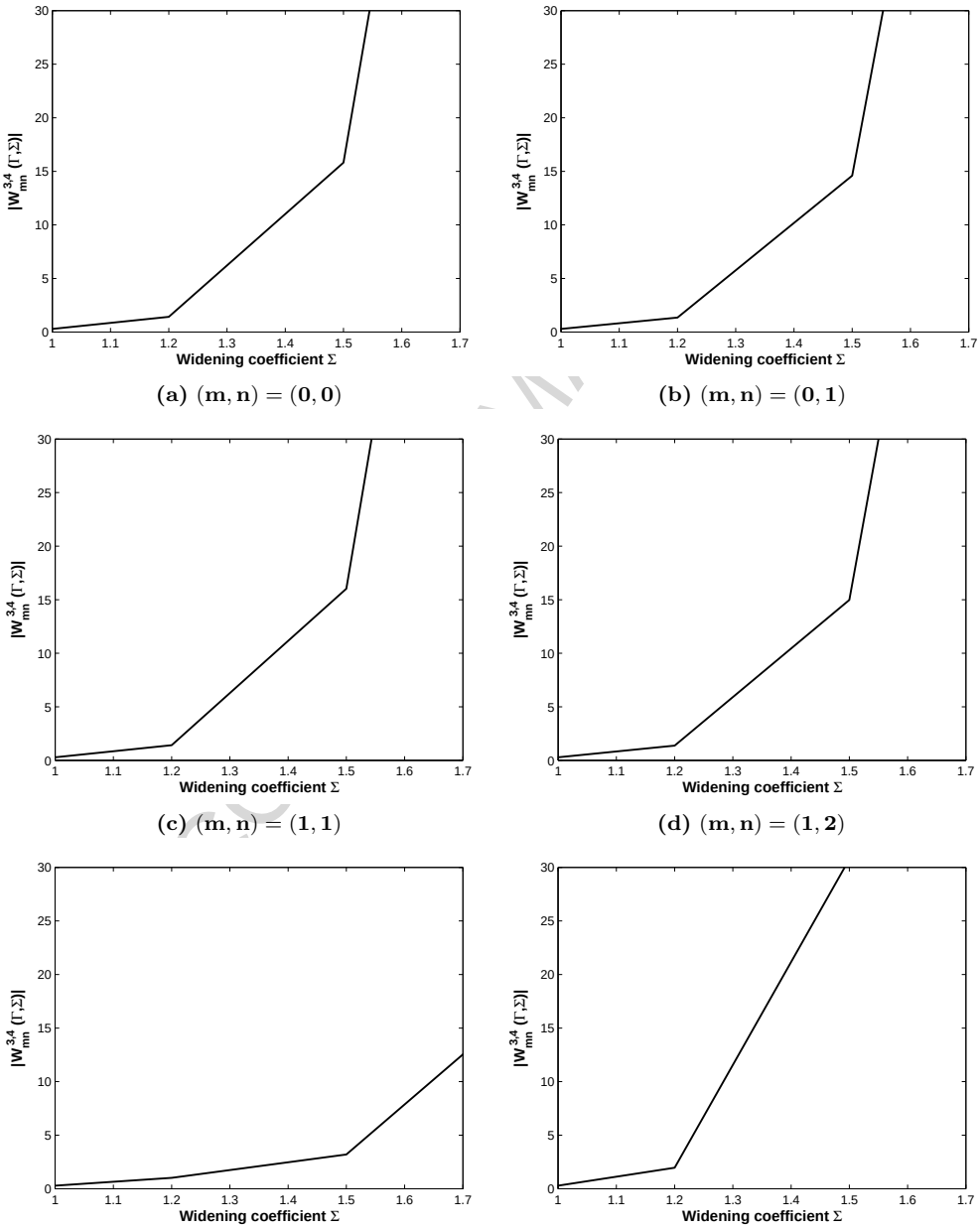

(a) $(\mathbf{m},\mathbf{n}) = (\mathbf{0},\mathbf{0})$ **(b)** $(\mathbf{m},\mathbf{n}) = (\mathbf{0},\mathbf{1})$

(c) $(\mathbf{m},\mathbf{n}) = (\mathbf{1},\mathbf{1})$ **(d)** $(\mathbf{m},\mathbf{n}) = (\mathbf{1},\mathbf{2})$

(e) $(\mathbf{m},\mathbf{n}) = (\mathbf{0},\mathbf{7})$ **(f)** $(\mathbf{m},\mathbf{n}) = (\mathbf{7},\mathbf{7})$

Fig. 4. Sensitivity of the Wronskian-like function $|W_{mn}^{3,4}(\Gamma,\Sigma)|$ given by Eq.(17) to the widening coefficient $\sigma = \dfrac{a_\Sigma}{a_\Gamma}$. Case where $e_\Gamma = e_\Sigma = 0.9$ and $ka_\Gamma = 10$.

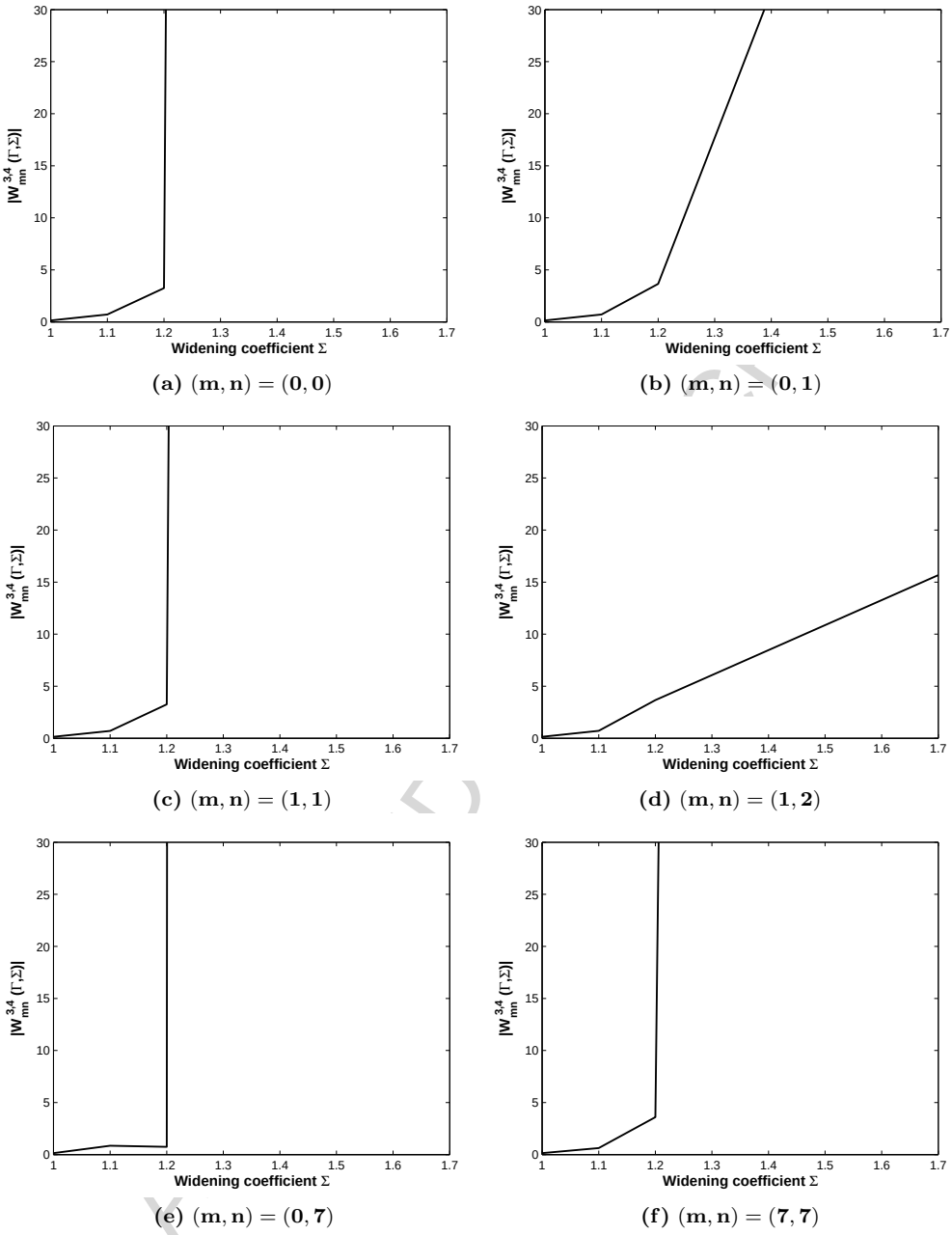

(a) $(\mathbf{m},\mathbf{n}) = (\mathbf{0},\mathbf{0})$ **(b)** $(\mathbf{m},\mathbf{n}) = (\mathbf{0},\mathbf{1})$

(c) $(\mathbf{m},\mathbf{n}) = (\mathbf{1},\mathbf{1})$ **(d)** $(\mathbf{m},\mathbf{n}) = (\mathbf{1},\mathbf{2})$

(e) $(\mathbf{m},\mathbf{n}) = (\mathbf{0},\mathbf{7})$ **(f)** $(\mathbf{m},\mathbf{n}) = (\mathbf{7},\mathbf{7})$

Fig. 5. Sensitivity of the Wronskian-like function $|W^{3,4}_{mn}(\Gamma,\Sigma)|$ given by Eq.(17) to the widening coefficient $\sigma = \dfrac{a_\Sigma}{a_\Gamma}$. Case where $e_\Gamma = e_\Sigma = 0.9$ and $ka_\Gamma = 20$.

3.2 Accuracy of the approximate scattered field

Next, we assess analytically the accuracy performance of the proposed approximate boundary condition in the high frequency regime. We study the asymptotic behavior of the Fourier coefficients of the solution of the *canonical*

boundary value problem for high wavenumber values, and present numerical results for illustration purposes. This analysis highlights the potential of the proposed local approximate DtN2 absorbing boundary condition for solving accurately acoustic scattering problems with elongated scatterers.

3.2.1 Mathematical results

We compare the approximate scattered field u^{DtN} given by Eq. (16) to the exact scattered field u^{scat} given by Eq. (11) by analyzing the asymptotic behavior of the Fourier coefficients given by Eq. (21) as $ka_\Gamma \to \infty$. The following result analyzes the asymptotic behavior of the propagating Fourier coefficients corresponding to the approximate scattered field u^{scat} given by Eq. (11). Recall that the first two modes in the infinite series given by Eq. (16) are the exact modes propagating towards the infinity and do not reflect at the artificial boundary Σ (see Eq. (24)). Therefore, the following analysis addresses the case of the remaining modes. To do this, we introduce the following set

$$\mathcal{N} = \Big\{(m,n) \in \mathbb{N}^2 \backslash \{(0,0),(0,1)\} \text{ such that } n \geq m\Big\} \tag{40}$$

Proposition 3.8 *For all $(m,n) \in \mathcal{N}$, the propagating Fourier coefficients d_{mn}^{DtN} given by Eq.*(21) *satisfy:*

$$d_{mn}^{\mathrm{DtN}} \sim d_{mn}^{\mathrm{scat}} \; ; \quad \text{as} \quad ka_\Gamma \to \infty \tag{41}$$

where d_{mn}^{scat} are the Fourier coefficients corresponding to the exact scattered field u^{scat} (see Eqs. (11)-(12)*).*

Proof of Proposition 3.8. In order to obtain the asymptotic behavior of the Fourier coefficients d_{mn}^{DtN} given by Eq. (21), we first derive the asymptotic behavior of the numerator $\Psi_{mn_{|\Sigma}}^{(4)} R_{mn_{|\Gamma}}^{(3)}$ where $\Psi_{mn_{|\Sigma}}^{(4)}$ is given by Eq. (18). To do this, we substitute into Eq. (18) the asymptotic behavior of (a) $R_{mn_{|\Sigma}}^{(4)}$ given by Eq. (27), (b) $r_{mn_{|\Sigma}}^{(4)}$ given by Eq. (30), and (c) $c_{mn_{|\Sigma}}$ given by Eq. (33). Then, as $ka_\Gamma \to \infty$, we obtain:

$$\Psi_{mn_{|\Sigma}}^{(4)} R_{mn_{|\Gamma}}^{(3)} \sim \frac{1}{ka_\Gamma\, ka_\Sigma}\, e^{\mathrm{i}\, k(a_\Gamma - a_\Sigma)} \left[-e_\Sigma ka_\Sigma \left(\mathrm{i} - \frac{1}{ka_\Sigma}\right) + e_\Sigma ka_\Sigma \left(-\mathrm{i} - \frac{1}{ka_\Sigma}\right)\right] \tag{42}$$

Proposition 3.8 is then an immediate consequence of substituting Eq. (25) (see Proposition 3.3) and Eq. (42) into Eq. (21).

□

Remark 3.9 *Proposition 3.8 indicates that* $\dfrac{\tau_{mn}^{\mathrm{DtN}}}{d_{mn}^{\mathrm{scat}}} \to 0$ *as* $ka_\Gamma \to \infty$. *This suggests that, for large values of the wavenumber ka_Γ, the propagating term*

of the approximate scattered field u^{DtN} *(see Eq. Eq.* (11)*) becomes a good approximation the exact scattered field* u^{scat}*.*

Next, we analyze the asymptotic behavior of the reflection Fourier coefficients τ_{mn}^{DtN} given by Eq. (21). The following result compares asymptotically τ_{mn}^{DtN} to the Fourier coefficients d_{mn}^{scat} corresponding to the exact scattered field u^{scat}.

Proposition 3.10 *For all* $(m,n) \in \mathcal{N}$*, the reflection Fourier coefficients* τ_{mn}^{DtN} *given by Eq.*(21) *satisfy:*

$$\tau_{mn}^{\mathrm{DtN}} \sim \frac{(-1)^{\mathrm{n}+1}}{2\,(ka_\Sigma)^2}\left(m-n+\frac{n(n+1)}{2}\right) e^{2\,\mathrm{i}\,ka_\Sigma}\, d_{mn}^{\mathrm{scat}}\;; \quad \text{as} \quad ka_\Gamma \to \infty \tag{43}$$

where d_{mn}^{scat} *are the Fourier coefficients corresponding to the exact scattered field* u^{scat} *(see Eqs.* (11)-(12)*).*

Proof of Proposition 3.10. In order to obtain the asymptotic behavior of the Fourier coefficients τ_{mn}^{DtN} given by Eq. (21), we first derive the asymptotic behavior of the numerator $\Psi_{mn_{|\Sigma}}^{(3)} R_{mn_{|\Gamma}}^{(3)}$ where $\Psi_{mn_{|\Sigma}}^{(3)}$ is given by Eq. (18). To do this, we substitute into we substitute into Eq. (18) the asymptotic behavior of (a) $R_{mn_{|\Sigma}}^{(3)}$ given by Eq. (27), (b) $r_{mn_{|\Sigma}}^{(3)}$ given by Eq. (30), and (c) $c_{mn_{|\Sigma}}$ given by Eq. (33). Then, we obtain:

$$\Psi_{mn_{|\Sigma}}^{(3)} R_{mn_{|\Gamma}}^{(3)} \sim \frac{-\,\mathrm{i}\,e_\Sigma}{ka_\Gamma\,(ka_\Sigma)^2}\left(m-n+\frac{n(n+1)}{2}\right) e^{\mathrm{i}\,(k(a_\Gamma+a_\Sigma)-(n+1)\pi)}\;; \quad \text{as} \quad ka_\Gamma \to \infty \tag{44}$$

Next, we substitute (25) (see Proposition 3.3) and Eq. (44) into Eq. (21). The, we obtain:

$$\tau_{mn}^{\mathrm{DtN}} \sim \frac{1}{2\,(ka_\Sigma)^2}\left(m-n+\frac{n(n+1)}{2}\right) e^{2\,\mathrm{i}\,ka_\Sigma}\, e^{-\mathrm{i}\,(n+1)\pi}\, d_{mn}^{\mathrm{scat}}\;; \quad \text{as} \quad ka_\Gamma \to \infty \tag{45}$$

which concludes the proof of Proposition 3.10.

□

Remark 3.11 *Proposition 3.10 suggests that, for large values of the wavenumber* ka_Γ*, the reflected waves in the approximate scattered field* u^{DtN} *(see Eq. Eq.* (11)*) become smaller (decay to zero) compared to the (propagating) exact scattered field* u^{scat}*.*

The next result indicates the rate of decay of the reflection Fourier coefficients τ_{mn}^{DtN} as $ka_\Gamma \to \infty$.

Theorem 3.12 *For all* $(m,n) \in \mathcal{N}$*, the reflection Fourier coefficients* τ_{mn}^{DtN} *given by Eq.*(21) *satisfy:*

$$\left|\tau_{mn}^{\mathrm{DtN}}\right| < \frac{2\,\kappa}{\pi^{1/4}} \left(\frac{n(n-1)}{2} + m\right) \left(\frac{e_\Gamma\, a_\Gamma}{a_\Sigma}\right)^{1/8} \frac{1}{(k a_\Sigma)^{15/8}}\ ; \quad \text{as} \quad k a_\Gamma \to \infty \tag{46}$$

where the positive constant κ *satisfies:*

$$\kappa \approx 1.086435 \tag{47}$$

The proof of Theorem 3.12 is based on the following intermediate result that provides an upper bound on the Fourier coefficients corresponding to the incident plane wave u^{inc} given by Eq. (8).

Lemma 3.13 *For all* $(m,n) \in \mathcal{N}$*, the Fourier coefficients* d_{mn}^{inc} *given by Eq.* (10) *satisfy:*

$$|d_{mn_{|\Gamma}}^{\mathrm{inc}}| < 4\,\kappa \left(\frac{\sqrt{e_\Gamma k a_\Gamma}}{\pi}\right)^{1/4}; \quad k a_\Gamma \to +\infty \tag{48}$$

where the positive constant κ *is given by Eq.* (47)*.*

Proof of Lemma 3.13. Recall that, as $k a_\Gamma \to +\infty$, the asymptotic behavior of the angular spheroidal wave function corresponding to the $(mn)^{\text{th}}$ mode is given by (see Eq. (3.251) p. 243 in [18]):

$$\begin{aligned} S_{mn}\left(e_\Gamma k a_\Gamma, \cos\varphi_0\right) \sim (-1)^m \left(\frac{4\sqrt{e_\Gamma k a_\Gamma}}{\pi}\right)^{1/4} \frac{1}{(n-m)!} \left(\frac{(n+m)!}{2n+1}\right)^{1/2} \\ .\,(1-\cos^2\varphi_0)^{m/2}\, D_{n-m}\left(\left(2\sqrt{e_\Gamma k a_\Gamma}\right)^{1/2} \cos\varphi_0\right) \end{aligned} \tag{49}$$

where $D_{n-m}\left(\left(2\sqrt{e_\Gamma k a_\Gamma}\right)^{1/2} \cos\varphi\right)$ are the parabolic cylinder functions [1]. These functions can be expressed in terms of the Hermite polynomials as follows (see Eq. (19.3.1) p. 687 and Eq. (19.13.1) p. 691 in [1]):

$$\begin{aligned} D_{n-m}\left(\left(2\sqrt{e_\Gamma k a_\Gamma}\right)^{1/2} \cos\varphi_0\right) = 2^{(m-n)/2}\, H_{n-m}\left((e_\Gamma k a_\Gamma)^{1/4} \cos\varphi_0\right) \\ .\,\exp(-\frac{\sqrt{e_\Gamma k a_\Gamma}\cos^2\varphi_0}{2}) \end{aligned} \tag{50}$$

Moreover, the Hermite polynomials satisfy (see Eq. (22.14.17) p. 786 in [1]):

$$\left|H_{n-m}\left((e_\Gamma k a_\Gamma)^{1/4} \cos\varphi_0\right)\right| < \kappa\, 2^{(n-m)/2} \sqrt{(n-m)!}\, \exp(\frac{\sqrt{e_\Gamma k a_\Gamma}\cos^2\varphi_0}{2}) \tag{51}$$

In addition, we have (see Eq. 3.23 p. 237 in [18]) that:

$$N_{mn} = \frac{2}{2n+1}\frac{(n+m)!}{(n-m)!} \tag{52}$$

Therefore, Eq. (48) results from substituting Eqs. (49)-(52) into Eq. (10).

□

Proof of Theorem 3.12. It follows from Eq. (43) that

$$|\tau_{mn}^{\mathrm{DtN}}| \sim \frac{1}{2\,(ka_\Sigma)^2}\left(\frac{n(n-1)}{2}+m\right)|d_{mn}^{\mathrm{scat}}|\;;\quad \text{as}\quad ka_\Gamma \to \infty \tag{53}$$

On the other hand, we have (see Eq. (21.9.4) p. 756 in [1]):

$$R^{(1)}_{mn_{|\Gamma}} \sim \Re(R^{(3)}_{mn_{|\Gamma}})\;;\quad ka_\Gamma \to +\infty \tag{54}$$

where $\Re(z)$ designates the real part of the complex number z.
Therefore, it follows from Eq. (13) and Eq. (54) that:

$$|d_{mn}^{\mathrm{scat}}| \sim \left|\cos\left(ka_\Gamma - \frac{1}{2}(n+1)\pi\right)\right| |d^{\mathrm{inc}}_{mn_{|\Gamma}}|\;;\quad ka_\Gamma \to +\infty \tag{55}$$

Eq. (46) results from substituting Eq. (48) and Eq. (55) into Eq. (53).

□

Remark 3.14 *The following four observations are noteworthy:*

i. Theorem 3.12 along with Proposition 3.8 prove that, as $ka_\Gamma \to \infty$ u^{DtN}*, the solution of the boundary value problem* (14)*, tends to the exact scattered field* u^{scat}*, the solution of the acoustic scattering problem* (7)*.*

ii. Theorem 3.12 states that the Fourier coefficients corresponding to the reflected modes decay faster than $\dfrac{1}{(ka_\Sigma)^{15/8}}$*. This quasi-quadratic decay of the reflected waves, for large wavenumber values ka, tends to indicate that the exterior boundary could be positioned at a very small distance from the surface of the scatterer while delivering an acceptable level of accuracy on the approximate scattered field* u^{DtN}*. This observation is illustrated numerically in the next paragraph (see Section 3.2.2).*

iii. The proof of estimate (46) *uses Taylor expansions and only one inequality (see Eq.* (51) *in the proof of Lemma 3.13) which is an estimate on Hermite polynomials (see Eq. (22.14.17) p. 786 in [1]). This proves that* (46) *is a sharp estimate. Nevertheless, there are a some reflected modes that decay much more faster than* $\dfrac{1}{(ka_\Sigma)^{15/8}}$*, as reported in [23]. More specifically, the*

modes u_{nm} *such that* $n \sim \sigma ka$ *and* $m << \dfrac{\sigma ka}{2e}$ *decay exponentially as* $ka \to \infty$ *(see Proposition B.2, Appendix B, in [23]) .*

iv. In the particular case where both Γ *and* Σ *are spherical-shaped boundaries, the reflection Fourier coefficients* τ_n^{BGT2} *corresponding to the BGT2 condition, satisfy (see Theorem A.3 in Appendix A):*

$$\left|\tau_n^{\mathrm{BGT2}}\right| < \frac{n(n+1)(2n+1)}{4}\,\frac{1}{(kR)^2}\;; \quad \text{as} \quad ka \to \infty \tag{56}$$

which is slightly better than the asymptotic behavior of τ_{mn}^{DtN} *in spite the fact that the proposed DtN2 boundary condition coincides with BGT2 on spherical-shaoed boundaries, as shown in [4],[23]. This result indicates that we cannot interchange the limit as* $e_\Sigma \to 0$ *with the limit as* $ka_\Sigma \to \infty$*.*

3.2.2 Numerical investigation of the accuracy

We assess numerically the accuracy of the local approximate DtN2 boundary condition given by Eq. (15) when applied in domain-based formulation for solving the *canonical*acoustic scattering problem given by (14).
Similarly to the previous numerical investigation (see Section 3.1.2), we perform this numerical investigation in the particular case where the two boundaries Γ and Σ are parallel. Hence, we assume that the semi-major and semi-minor axes satisfy respectively $a_\Sigma = \sigma\, a_\Gamma$ and $b_\Sigma = \sigma\, b_\Gamma$. The positive real number σ, called the *widening* coefficient, satisfies $\sigma \geq 1$. Recall that such an assumption implies that the two boundaries have the same eccentricity, that is $e_\Sigma = e_\Gamma = e$. We analyze the sensitivity of the accuracy to the value of σ, that is the position of the exterior boundary Σ with respect to the boundary Γ of the prolate spheroidal-shaped scatterer Ω. This is achieved by computing the 2-norm of (a) the reflection Fourier coefficients τ_{mn}^{DtN} given by Eq. (21) as a function of the distance between the interior boundary Γ and the artificial boundary Σ , i.e.

$$\sigma \longrightarrow \left(\sum_{m=0}^{+\infty}\sum_{n=m}^{+\infty} |\tau_{mn}^{\mathrm{DtN}}|^2\right)^{1/2}$$

and (b) the relative error between the approximate solution u^{DtN} given by Eq. (16) and the scattered filed u^{scat} given by Eq. (11) as a function of σ, i.e.

$$\sigma \longrightarrow \frac{\left(\sum_{m=0}^{+\infty}\sum_{n=m}^{+\infty}\left(|d_{mn}^{app} - d_{mn}^{scat}|^2 + |\tau_{mn}^{app}|^2\right)\right)^{1/2}}{\left(\sum_{m=0}^{+\infty}\sum_{n=m}^{+\infty}|d_{mn}^{scat}|^2\right)^{1/2}}$$

The goal in part (a) is to measure the intensity of the reflected waves, and

therefore to assess the level of transparency of the proposed boundary condition, whereas in part (b) we evaluate the accuracy as a function of the distance between the two boundaries. We compare the performance of this condition to the performance of the so-called BGT2 boundary condition designed in spherical coordinates in [6] and expressed in prolate spheroid coordinates in [21]. Note that the expression of Fourier coefficients $\mathrm{d}_{mn}^{\mathrm{BGT2}}$ and $\tau_{mn}^{\mathrm{BGT2}}$ corresponding to BGT2 condition can be found in [5] (see Eqs. (63)-(64), p. 34 in the INRIA technical report [5]). For illustration purpose, we present the results of two sets of numerical experiments performed where we have set $ka = 10$ and 20. These results have been obtained for two eccentricity values $e_\Sigma = e_\Gamma = 0.1$ corresponding to a prolate spheroid "close" to a sphere, and 0.9 corresponding to a "very" elongated regular prolate-spheroid boundary. The results depicted in Figs. (6)-(9) are obtained for an incident angle $\varphi_0 = \dfrac{\pi}{4}$. Note that the results for other incident directions are comparable [23]. The following observation are noteworthy:

- Figs. (6)-(7) indicate that the proposed DtN2 boundary condition given by Eq. (15) produces "little" reflections, especially for large eccentricity values. More specifically, for large eccentricity values ($e = 0.9$), the 2-norm of the reflection coefficients is already below 1% as soon as $\sigma > 1.2$, which corresponds to a small computational domain Ω^b. This result illustrate the high level of transparency of the proposed DtN2 boundary condition when applied on very elongated boundaries. On the other hand, for small eccentricity values corresponding to boundaries close to sphere ($e = 0.1$), the 2-norm of the reflection coefficients remains of order 5% for all frequencies even when the exterior boundary Σ is placed very far from the boundary Γ of the scatterer Ω, i.e. for large values of σ.
- The results depicted Figs. (8)-(9) indicate that proposed DtN2 boundary condition delivers the solution with a high level of accuracy. Indeed, for large eccentricity values ($e = 0.9$), the relative error, in the 2-norm sense, is below 0.1% as soon as $\sigma > 1.2$, which corresponds to a small computational domain Ω^b. This observation suggests that the proposed DtN2 boundary condition is very efficient when applied on very elongated boundaries. Observe that, for small eccentricity values ($e = 0.1$), the DtN2 boundary condition retains a good level of accuracy, the relative error is of order 1% when $\sigma > 1.4$ which corresponds to a relatively small computational domain.
- Figs. (6)-(9) show that the proposed DtN2 boundary condition given by Eq. (15) outperforms the BGT2 boundary condition when expressed in prolate spheroid coordinates in [21]. This superiority is more noticeable for small eccentricity values which is surprising because when $e \to 0$ both conditions tend to the same boundary condition.

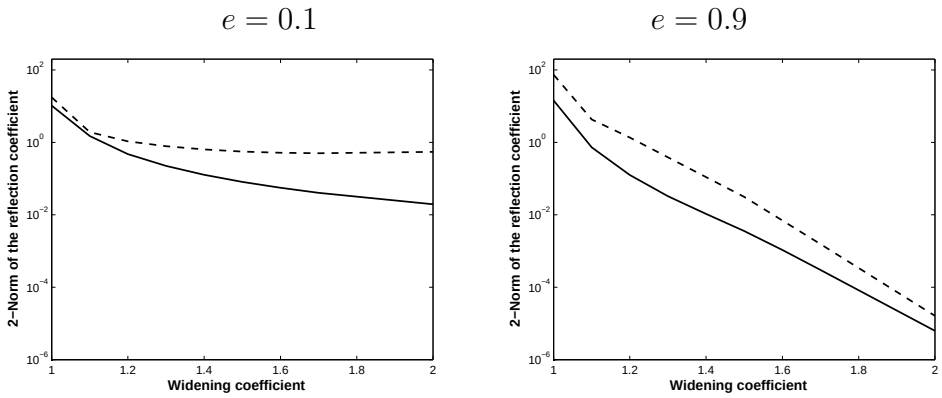

Fig. 6. Sensitivity of the reflection coefficients to the widening parameter σ for $ka = 10$ and incident angle $\varphi_0 = \frac{\pi}{4}$: DtN2 (plain), BGT2 (dashed).

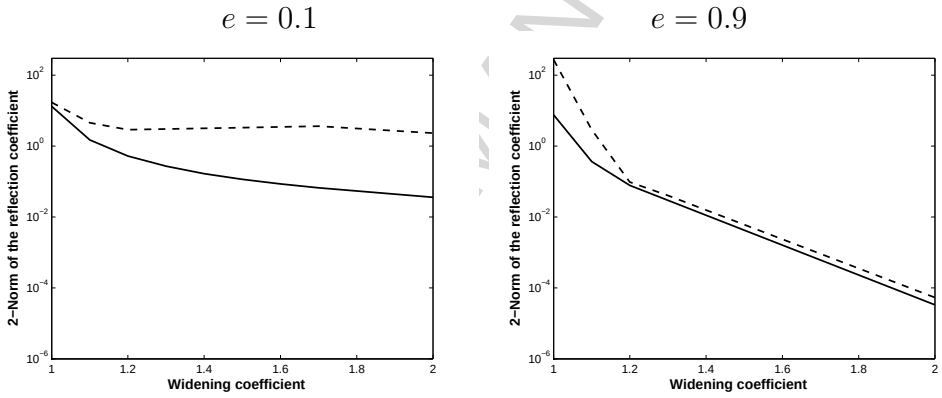

Fig. 7. Sensitivity of the reflection coefficients to the widening parameter σ for $ka = 20$ and incident angle $\varphi_0 = \frac{\pi}{4}$: DtN2 (plain), BGT2 (dashed).

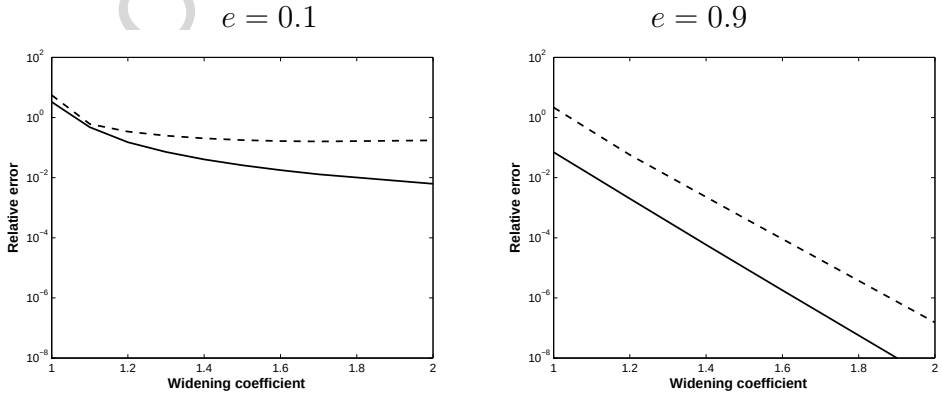

Fig. 8. Sensitivity of the relative error to the widening parameter σ for $ka = 10$ and incident angle $\varphi_0 = \frac{\pi}{4}$: DtN2 (plain), BGT2 (dashed).

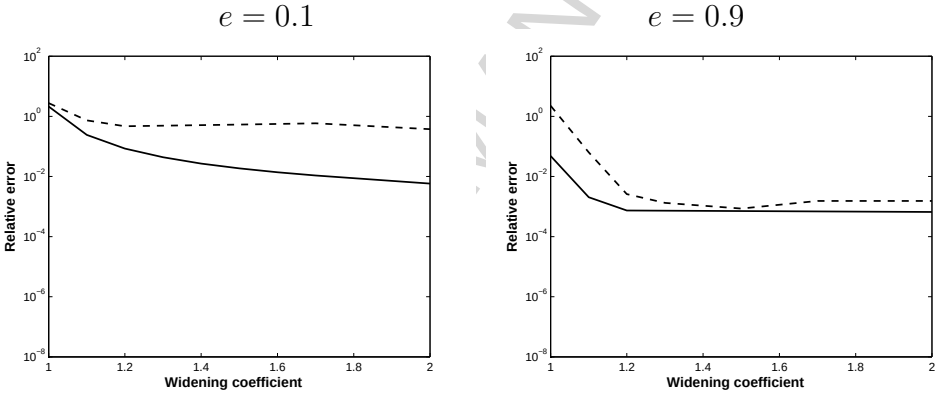

Fig. 9. Sensitivity of the relative error to the widening parameter σ for $ka = 20$ and incident angle $\varphi_0 = \frac{\pi}{4}$: DtN2 (plain), BGT2 (dashed).

4 Conclusion

We have perfomed an analytical study of the performance of the local approximate DtN2 absorbing boundary condition designed for exterior artificial prolate spheroidal-shaped boundaries that is well-suitable for elongated scatterers [4]. We have adopted a domain-based formulation to conduct this analysis in the high frequency regime. The mathematical analysis of the approximate scattered field, i.e. the solution of the *canonical* boundary value problem, proves that the DtN2 produces reflections at the exterior boundary that decay faster than $1/(ka_\Gamma)^{15/8}$, while the propagating waves tend to the exact scattered field. The numerical investigation of the relative error for the considered boundary value problem reveals that it is enough to set the widening coefficient σ at about 1.2 to retain a level of accuracy less than 1%. These two observations tend to indicate that, in practice, the use of the DtN2 boundary condition on a prolate spheroidal-shaped boundary surrounding the smallest prolate spheroid that contains the considered elongated scatterer, incurs relatively small computation domain, in order to achieve an acceptable level of accuracy when solving high frequency acoustic scattering porblems. Recall that, in the low frequency regime, we have already demonstrated in [4] that the proposed absorbing boundary condition retains a good level of accuracy regardless of the slenderness of the boundary. This result was established using the OSRC formulation, which is an extreme case scenario since the use of a domain-based formulation would be less "demanding" on the boundary condition. Consequently, this study along with the previous one [4] illustrate the potential of the proposed absorbing boundary condition for solving efficiently acoustic scattering problems with elongated scatterers for all frequency regime. Furthermore, as stated earlier in the Introduction section, this absorbing boundary condition is exact for the first two modes, easy to implement and parallelize, and it retains the local structure of the computational scheme. These features make the proposed DtN2 boundary condition even more appealing.

Acknowledgments

The authors acknowledge the support by INRIA/CSUN Associate Team Program and by ANR/AHPI research program (Agence Nationale de la Recherche/ Analyse Harmonique et Problèmes Inverses). Any opinions, findings, conclusions or recommendations expressed in this material are those of the authors and do not necessarily reflect the views of ANR, CSUN, or INRIA.

Appendix

A Performance of the BGT2/DtN2 for spherical-shaped boundaries: Analytical results

We consider in this section the limit case where the eccentricity e becomes 0, that is, when the DtN2 boundary condition given by Eq.(15) coincides with the local DtN2 boundary condition given in [12] (see also Eq. (11), p. 19 in [13]). We recall that, unlike the two-dimensional case, the absorbing boundary conditions BGT2 and DtN2 are *identical* when employed on a sphere (see Proposition 3.2.1 p. 20 in [13]).

The goal of this study is to determine analytically the asymptotic behavior of the the reflection coefficients corresponding to the acoustic reflected waves produced by the BGT2/DtN2 boundary condition when employed on a spherical-shaped exterior boundary. To do this, we consider throughout this section the spherical coordinates (ξ, θ, φ) where r is the radius and θ, φ are the two Euler angles satisfying $x = r\sin\theta\cos\varphi$, $y = r\sin\theta\sin\varphi$, and $z = r\cos\theta$. We assume the sound-soft scatterer Ω to be a sphere of radius a, and the incident plane wave u^{inc} to be along the positive z-axis, i.e. $u^{\text{inc}} = e^{\mathrm{i}\,k\,\cos\theta}$ which can be expanded as (see, for example, Eq. 2.1.17, p. 28 in [14] or Eq. 2.6.99, p. 98 in [19]):

$$u^{\text{inc}} = \sum_{m=0}^{+\infty} d_n^{\text{inc}}\, j_n(kr)\, P_n(\cos\theta) \tag{57}$$

where the n^{th} Fourier coefficient d_n^{inc} is given by:

$$d_n^{\text{inc}} = \mathrm{i}^n\,(2n+1) \tag{58}$$

Note that j_n is the n-order spherical Bessel function of the first kind (see Eq. 10.1.1, p. 437 in [1]) and P_n is the Legendre polynomial of order n (see Eq. 8.6.18, p. 334 in [1]). Observe that these polynomials satisfy (see, for example, Eq. (70), p. 29 in [13]):

$$\frac{d}{d\theta}\left(\sin\theta\,\frac{d(P_n(\cos\theta))}{d\theta}\right) + n(n+1)\sin\theta\,P_n(\cos\theta) = 0 \tag{59}$$

It is well known (see, for example, Eq. (3.29), p. 52 in [8]) that the sound-soft acoustic scattered field (the solution of the boundary value problem given by Eq.(7)) can be expressed as follows

$$u^{\text{scat}} = \sum_{m=0}^{+\infty} d_n^{\text{scat}}\, h_n^{(1)}(kr)\, P_n(\cos\theta) \tag{60}$$

where the n^{th} Fourier coefficient d_n^{scat} is given by:

$$d_n^{\text{scat}} = -\,\mathrm{i}^n\,(2n+1)\,\frac{j_n(ka)}{h_n^{(1)}(ka)} \tag{61}$$

and $h_n^{(1)}$ is the n-order spherical Hankel function of the first kind (see Eq. 10.1.1, p. 437 in [1]).

Next, we consider the acoustic scattering problem formulated in a bounded domain Ω^b (see BVP(14)). As depicted in Fig.10, the bounded domain Ω^b is located outside the sphere of radius a, and inside the sphere of radius R, with $R \geq a$ and Σ being surface of the outer sphere. Moreover, the second boundary condition in BVP(14), the Robin-type boundary condition on Σ, is replaced by the BGT2/DtN2 boundary condition (see, for example, Eq. (8), p. 19 in [13]), that is:

$$\frac{\partial u}{\partial r} = \left(\mathrm{i}k - \frac{1}{R}\right) u + \frac{1}{2R(1-\mathrm{i}kR)}\,\Delta_\Sigma u \tag{62}$$

where the Laplace-Beltrami operator Δ_Σ is defined by;

$$\Delta_\Sigma u = \frac{1}{\sin\theta}\,\frac{\partial}{\partial\theta}\left(\sin\theta\,\frac{\partial u}{\partial\theta}\right) + \frac{1}{\sin^2\theta}\,\frac{\partial^2 u}{\partial\varphi^2} \tag{63}$$

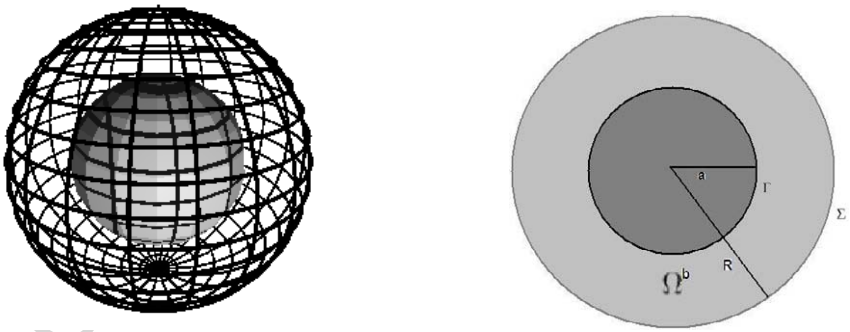

Fig. 10. Geometry of the bounded computational domain Ω^b (left) with a two-dimensional illustration in the xy-plane (right).

Consequently, the solution of the resulting boundary value problem, u^{DtN2}, can be expanded as follows:

$$u^{\text{BGT2}} = \sum_{m=0}^{+\infty} \left(d_n^{\text{BGT2}}\,h_n^{(1)}(kr) + \tau_n^{\text{BGT2}}\,h_n^{(2)}(kr)\right)\,P_n(\cos\theta) \tag{64}$$

where $h_n^{(2)}$ is the n-order spherical Hankel function of the second kind (see Eq. 10.1.1, p. 437 in [1]). Note that the outgoing/propagating modes are represented by $h_n^{(1)}(kr)$ and the incoming/reflected modes are characterized with $h_n^{(2)}(kr)$.

Next, we investigate analytically the asymptotic behavior of the reflection Fourier coefficients τ_n^{BGT2} corresponding to the reflected waves as $ka \to \infty$. First, we introduce first for all $n \in \mathbb{N}$, the following wronskian-like expression:

$$W_n(a,R) = h_n^{(1)}(ka)\,\varphi_n^{(2)}(kR) - h_n^{(2)}(ka)\,\varphi_n^{(1)}(kR) \tag{65}$$

where

$$\varphi_n^{(j)}(kR) = k\,h_n^{(j)'}(kR) - \gamma_n\,h_n^{(j)}(ka)\;; \quad j = 1,2 \tag{66}$$

and

$$\gamma_n = \mathrm{i}k - \frac{1}{R} - \frac{n(n+1)}{2R(1-\mathrm{i}kR)}\;; \quad j = 1,2 \tag{67}$$

Second, we state the necessary and sufficient condition for the existence and the uniqueness of the solution u^{BGT2}, and we give the explicit expression of the corresponding Fourier coefficients.

Proposition A.1 *The approximate scattered field u^{BGT2} given by Eq.*(64) *exists and is unique if and only if*

$$W_n(a,R) \neq 0 \quad \forall\, n \in \mathbb{N} \tag{68}$$

Moreover, if condition (68) *is satisfied, then for all $n \in \mathbb{N}$, the Fourier coefficients d_n^{BGT2} and τ_n^{BGT2} are given by:*

$$\begin{cases} d_n^{\mathrm{BGT2}} = -\dfrac{\varphi_n^{(2)}(kR)\,j_n(ka)}{W_n(a,R)}\,d_n^{\mathrm{inc}} \\[2ex] \tau_n^{\mathrm{BGT2}} = \dfrac{\varphi_n^{(1)}(kR)\,j_n(ka)}{W_n(a,R)}\,d_n^{\mathrm{inc}} \end{cases} \tag{69}$$

Proof of Proposition A.1. It follows from Eq.(59), Eqs.(62)-(64), and Eq.(67)that:

$$\begin{cases} d_n^{\mathrm{BGT2}} h_n^{(1)}(ka) + \tau_n^{\mathrm{BGT2}} h_n^{(2)}(ka) = -d_n^{\mathrm{inc}}\, j_n(ka) \\[2ex] d_n^{\mathrm{BGT2}} k\, h_n^{(1)'}(kR) + \tau_n^{\mathrm{BGT2}} k\, h_n^{(2)'}(kR) = \gamma_n \left(d_n^{\mathrm{BGT2}} h_n^{(1)}(kR) + \tau_n^{\mathrm{BGT2}} h_n^{(2)}(kR) \right) \end{cases} \tag{70}$$

We then conclude the proof by solving the 2×2 linear system (70) and using Eqs.(65)-(66).

□

Remark A.2 *Observe that $d_n^{\mathrm{BGT2}} = d_n^{\mathrm{scat}}$ and $\tau_n^{\mathrm{BGT2}} = 0$ for $n = 0, 1$, which is expected since, by construction, the absorbing boundary condition BGT2/DtN2 is exact for the first two modes.*

Finally, we state the main result of this section. It describes the asymptotic behavior of the reflection Fourier coefficients τ_n^{BGT2} ($n \geq 2$), corresponding to the reflected waves, as $ka \to \infty$.

Theorem A.3 *For all $n \geq 2$, the reflection Fourier coefficient τ_n^{BGT2} given by Eq.*(69) *satisfies:*

$$\left|\tau_n^{\mathrm{BGT2}}\right| < \frac{n(n+1)(2n+1)}{4}\,\frac{1}{(kR)^2}\;; \quad \text{as} \quad ka \to \infty \tag{71}$$

The Proof of Theorem A.3 is based on the following intermediate result.

Lemma A.4 *For all $n \geq 2$, the wronskian-like expression $W_n(a,R)$ given by Eq.* (65) *satisfies:*

$$W_n(a,R) \sim \frac{1}{kaR}\left[\frac{n(n+1)}{k}\left(\frac{1}{a}-\frac{1}{R}\right) - 2\mathrm{i}\right] e^{\mathrm{i}\,k(a-R)}\;; \quad \text{as} \quad ka \to \infty \tag{72}$$

Proof of Lemma A.4. We know (see, for example, Eq. (82), p. 31 in [13]) that:

$$h_n^{(1)}(kR) = \overline{h_n^{(2)}(kR)} \sim \frac{(-1)^n}{kR}\left(\frac{n(n+1)}{2kR} - \mathrm{i}\right) e^{\mathrm{i}\left(kR+\frac{n\pi}{2}\right)}\;; \quad \text{as} \quad ka \to \infty \tag{73}$$

Hence, it follows from Eqs.(66)-(67), and Eq.(73) that:

$$\varphi_n^{(1)}(kR) \sim \frac{(-1)^n}{R}\,\frac{n(n+1)}{2(kR)^2}\left(1 + -\mathrm{i}\frac{(n-1)(n+2)}{2kR}\right) e^{\mathrm{i}\left(kR+\frac{n\pi}{2}\right)}\;; \quad \text{as} \quad ka \to \infty \tag{74}$$

and

$$\varphi_n^{(2)}(kR) \sim \frac{(-1)^n}{R}\left(2 - \mathrm{i}\frac{n(n+1)}{kR}\right) e^{-\mathrm{i}\left(kR+\frac{n\pi}{2}\right)}\;; \quad \text{as} \quad ka \to \infty \tag{75}$$

Therefore, the asymptotic behavior (72) results from substituting Eqs.(73)-(75) into Eq.(65).

□

Remark A.5 *Observe that Lemma A.4 proves that the necessary and sufficient condition* (68) *is fullfilled in the high frequency regime. Hence, the boundary value problem* (14) *admits a unique solution u^{BGT2} in the high frequency regime regardless of the location of the artificial boundary Σ.*

Proof of Theorem A.3. Using (73), we deduce that:

$$j_n(ka) = \Re(h_n^{(1)}(ka)) \sim \frac{(-1)^n}{ka}\left[\frac{n(n+1)}{2ka}\cos\left(ka+\tfrac{n\pi}{2}\right) + \sin\left(ka+\tfrac{n\pi}{2}\right)\right] \; ; \quad \text{as} \quad ka \to \infty \tag{76}$$

Then, estimate (71) given in Theorem A.3 is an immediate consequence of substituting Eq. (74), Eq. (76), Eq. (58), and Eq. (72) into Eq. (69).

□

References

[1] M. Abramovitz, I. Stegun, *Handbook of Mathematical Functions with Formulas, Graphs and Mathematical Tables*, Dover Publications, New York, 1972.

[2] X. Antoine, *Fast approximate computation of a time-harmonic scattered field using the On-Surface Radiation Condition method*, IMA J. Appl. Math., 66 (1), 83–110, 2001.

[3] X. Antoine, M. Darbas, Y.Y. Lu, *An improved surface radiation condition for high-frequency acoustic scattering problems*, Comput. Methods Appl. Mech. Engrg., 195 (33-36), 4060–4074, 2006.

[4] H. Barucq, R. Djellouli, A. Saint-Guirons, *Performance assessment of a new class of local absorbing boundary conditions for elliptical-shaped boundaries*, Applied Numerical Mathematics, 59, 1467–1498, 2009.

[5] H. Barucq, R. Djellouli, A. Saint-Guirons, *High frequency analysis of the efficiency of a local approximate DtN2 boundary condition for prolate spheroidal-shaped boundaries*, INRIA Research Report, No.7137 (2009). Available online at: http://hal.inria.fr/inria-00438845/fr/.

[6] A. Bayliss, M. Gunzburger, E. Turkel, *Boundary conditions for the numerical solution of elliptic equations in exterior regions*, SIAM J. Appl. Math., 42 (2), 430–451, 1982.

[7] J.J. Bowman, T.B.A. Senior, P.L.E. Uslenghi, *Electromagnetic and acoustic scattering by simple shapes*, North-Holland Publishing company, Amsterdam, 1969.

[8] D. Colton, R. Kress, *Inverse Acoustic and Electromagnetic Scattering Theory*, Applied Mathematical Sciences 93, Springer-Verlag, New York, 1998.

[9] M. Darbas, *Préconditionneurs analytiques de type Calderon pour les formulations intégrales des problèmes de diffraction d'ondes*, Thèse de Doctorat, Université de Toulouse 1 et Toulouse 3, INSA Toulouse, 2004.

[10] C. Flammer, *Spheroidal Functions*, Standford University Press, Standford, CA, 1957.

[11] D. Givoli and J.B. Keller, *Nonreflecting boundary conditions for elastic waves*, Wave Motion, 12(3), 261–279, 1990.

[12] I. Harari, T.J.R. Hughes, *Analysis of continuous formulations underlying the computation of time-harmonic acoustics in exterior domains*, Comput. Methods Appl. Mech. Engrg., 97 (1), 103–124, 1992.

[13] I. Harari, R. Djellouli, *Analytical study of the effect of wave number on the performance of local absorbing boundary conditions for acoustic scattering*, Applied Numerical Mathematics, 50, 15-47, 2004.

[14] F. Ihlenburg, *Finite Element Analysis of Acoustic Scattering*, Applied Mathematical Sciences 132, Springer-Verlag, New York, 1998.

[15] G.A. Kriegsmann, A. Taflove, K.R. Umashankar, *A new formulation of electromagnetic wave scattering using an on-surface radiation boundary condition approach*, IEEE Trans. Antennas and Propagation, 35 (2), 153–161, 1987.

[16] F. Magoulès, *Computational Methods for Acoustics Problems*, Saxe-Coburg Publications, 2008.

[17] M. Medvinsky, E. Turkel, U. Hetmaniuk, *Local absorbing boundary conditions for elliptical shaped boundaries*, J. Comput. Phys., 47 (1), 575–595, 2008.

[18] J. Meixner, F.W. Schafle, *Matieusche funktionen and spharoidfunktionen*, Springer Verlag, Berlin, 1954.

[19] J. C. Nédélec, *Acoustic and Electromagnetic Equations, Integral Representation for Harmonic Problems*, Applied Mathematical Sciences 144, Springer-Verlag, New York, 2001.

[20] M. Nigsch, *Numerical studies of time-independent and time-dependent scattering by several elliptical cylinders*, Journal of Computational and Applied Mathematics, 204, 231-241, 2007.

[21] R.C. Reiner, R. Djellouli, I. Harari, *The performance of local absorbing boundary conditions for acoustic scattering from elliptical shapes*, Comput. Methods Appl. Mech. Engrg, 195, 3622-3665, 2006.

[22] R.C. Reiner, R. Djellouli, *Improvement of the performance of the BGT2 condition for low frequency acoustic scattering problems*, Wave Motion, 43, 406–424, 2006.

[23] A-G. Saint-Guirons, *Construction et analyse de conditions absorbantes de type Dirichlet-to-Neumann pour des frontières ellipsoïdales*, Thèse de Doctorat, Université de Pau et des Pays de l'Adour, 2008.

[24] E. Turkel, *Boundary Conditions and Iterative Schemes for the Helmholtz Equation in Unbounded Regions*, In: Computational Methods for Acoustics Problems, F. Magoulès (ed.), Saxe-Coburg Publications, , 127–158, 2009 .